2018-09-06

Crack tip plastic zone evolution during an overload cycle and the contribution of plasticity-induced shielding to crack growth rate changes

Vasco-Olmo, JM

10.1111/ffe.12840
Fatigue and Fracture of Engineering Materials and Structures
Wiley

Crack tip plastic zone evolution during an overload cycle and the contribution of plasticity-induced shielding to crack growth rate changes

J.M. Vasco-Olmo[1], F.A. Díaz[1], M.N. James[2, 3], Bing Yang[2, 4]

[1]Departamento de Ingeniería Mecánica y Minera, University of Jaén, Jaén, Spain.

[2]School of Marine Science & Engineering, University of Plymouth, Plymouth, England.

[3]Department of Mechanical Engineering, Nelson Mandela Metropolitan University, Port Elizabeth, South Africa.

[4]State Key Laboratory of Traction Power, Southwest Jiaotong University, Chengdu, China

Abstract

This work explores the contribution to crack growth rate acceleration and deceleration that arises from plasticity-induced shielding during an overload cycle. The CJP model of crack tip displacements and stress fields [1] was proposed in order to better capture the influences on the applied elastic stress field of the plastic enclave that is generated around a growing fatigue crack. The model does this through a set of elastic stresses applied at a notional elastic-plastic boundary, and it has been shown to accurately model plastic zone shape and size [2], whilst its ability to predict the effective range of stress intensity factor during a fatigue cycle has been independently verified [3]. In this paper the CJP model is used to follow plastic zone size and shape through an overload fatigue cycle and to assess the extent that plasticity-induced shielding accounts for the observed crack growth changes. The changes in effective stress intensity factor range during the overload demonstrate that the observed growth rate changes during overload cycles can only be partially rationalised through plasticity-induced shielding (closure).

Keywords: crack tip plastic zone, overloads, crack tip displacement fields, plasticity-induced shielding, fatigue.

Nomenclature:

A', B', C', E', F':	coefficients in the CJP model for describing crack tip displacements fields
A_{PZ}:	area of the plastic zone
a:	crack length
da/dN:	fatigue crack growth rate
G:	shear modulus
i:	square root of -1
K_F:	stress intensity factor driving crack growth in the CJP model
K_I:	mode I stress intensity factor
K_R:	stress intensity factor acting to retard crack growth
K_S:	stress intensity factor acting in the shear direction along the crack flanks at the elastic-plastic interface
R:	ratio between the minimum and the maximum applied load in fatigue
r, θ:	polar coordinates
T:	T-stress
u, v:	components of the displacement vector
E:	Young's modulus
z:	complex coordinate around the crack tip
ΔK:	stress intensity factor range
ε_{xx}, ε_{yy}, ε_{xy}:	strain fields
κ:	function of Poisson's ratio
ν:	Poisson's ratio
σ_x, σ_y, τ_{xy}:	stress components in Cartesian coordinates

1. Introduction

Simultaneous determination of plastic zone size and shape at the tip of a growing fatigue crack is recognised in the fracture mechanics and fatigue community as a relatively difficult problem, and is a contributory factor to the ongoing uncertainty around plasticity-induced shielding and its real contribution to observed crack growth rate effects arising from overload cycles during fatigue. A significant body of research work has therefore endeavoured to quantify the crack tip plastic zone both numerically and experimentally. The experimental techniques include microhardness measurements, etching, optical interference, the use of microstrain gauges and electron microscopy [4]. More advanced experimental techniques, such as synchrotron X-ray

diffraction [5] and tomography [6], digital image correlation (DIC) [7], thermoelastic stress analysis (TSA) [8] and electron backscatter diffraction (EBSD) [9]–[11] have started to be applied to the quantitative measurement of plastic strain fields during fatigue crack growth and hence to characterising the plastic zone at the crack tip.

For example, James et al [5] reported one of the first uses of synchrotron X-ray diffraction to measure the strains in the x and y-directions at the tip of a crack in an aluminium CT specimen under applied loads equal to the minimum and maximum loads in the prior fatigue cycling and compare the results with those obtained by numerical modelling. Their work demonstrated the capability of the technique although the data suffered from resolution problems. Several years later, using a more advanced instrument, Steuwer et al [6] performed similar work using synchrotron X-ray diffraction and tomography to map the two dimensional strain field around a crack tip and also compared their results with predictions from numerical analysis. They compared the experimental results for the transverse strain profile (perpendicular direction to the crack wake) with numerical results using the software Abaqus. This comparison considered three keys features: the 'lobes' of strain ahead of the crack tip, the strain concentration in the overloaded region just behind the tip and the compressive field adjacent to the crack wake. Zhang and Liu [7] used DIC to determine the loading and unloading strain fields during cyclic loading of Al7075-T6 alloy by taking photographs of the crack tip region during step-wise fatigue loading. The plastic zone size was obtained by combining the DIC results with the material constitutive relationship.

Patki and Patterson [8] have used thermoelastic stress analysis (TSA) to measure the size of the crack tip plastic zone and investigated the effects of plasticity-induced crack closure and overloads in a 2024 aluminium alloy. A Muskhelishvili-type description of the crack tip stress fields was used to calculate stress intensity factors during crack growth. In addition, they proposed a new method to directly measure the extent of the crack tip plastic zone based on the phase difference between TSA and the applied load. Measurements of the crack tip plastic zone were correlated with changes in the stress intensity factor derived from TSA data, during

constant amplitude loading as well as after single and multiple overloads. Immediately post-overload they measured an increase in the plastic zone of up to 50%, while the stress intensity factor range and the crack growth rate decreased until the crack had grown through the overload plastic zone and crack growth rates had returned to their pre-overload level.

Quantitative measurements of plastic strain field can also be made using backscattered electron imaging or diffraction (EBSD) techniques [10], [11]. Yang et al [10] introduced a novel approach of applying a discrete Fourier transform (DFT) to backscattered electron (BSE) images of the plastic crack tip zone in order to map the mesoscale plastic strain distribution resulting from heterogeneous plastic deformation under multiaxial loading in engineering components. Similar work by Carroll et al [11] made quantitative full-field measurements of plastic strain near a growing fatigue crack using a DIC technique based on EBSD microstructural data on grain shape and orientation. They observed that the accumulated plastic strain associated with fatigue crack growth exhibited inhomogeneity at two length scales. At the macroscale level the plastic wake contained asymmetric lobes of high strain associated with past crack tip zones, while high resolution DIC revealed inhomogeneities at the grain and sub-grain scale, with effective strain varying both from grain-to-grain and also within grains. Carroll et al [11] concluded that a better understanding of these multiscale heterogeneities could help explain variations in fatigue crack growth rate and crack path and could improve the understanding of fatigue crack closure and fracture in ductile metals.

Alongside these endeavours, a significant amount of work has also been directed towards measuring and understanding crack tip shielding mechanisms [12], [13] during fatigue crack growth under constant amplitude (CA) loading. Although such work has contributed to an improved understanding of plasticity-induced shielding, the precise mechanisms causing the observed changes in fatigue crack growth rate during overloads have remained unclear. Part of the problem arises with measurements of the effective range of stress intensity that are generally based on indirect experimental measurements; this complicates interpretation of the results and obscures understanding of the physical mechanisms involved. A number of these difficulties

were discussed many years ago in a paper by James [14]. The net result is that, at present, in variable amplitude loading (e.g. after the application of an overload), there is still controversy around the mechanisms responsible for the temporary retardations and accelerations observed in the fatigue crack growth rate [15] and their correlation with plasticity-induced closure. Measurements of shielding, or closure, are highly variable and accurate predictions of fatigue crack growth rate cannot easily be made. Although techniques like TSA may provide a value for the effective stress intensity factor, at least in certain alloys, they do not shed any light on the underlying mechanisms involved in plasticity-induced shielding

Under constant amplitude loading the plastic zone steadily increases in size as a function of crack length, and the application of an overload produces an instantaneous increase in the size of the plastic zone and, usually, a transient increase in crack growth rate, often followed by delayed retardation. It has been proposed that when an overload is applied, there is an initial increase in crack growth rate and retardation then occurs as the crack propagates through the enlarged plastic zone generated during the overload [16]–[18].

The present work applies overloads to growing fatigue cracks and uses the CJP model to identify accurate values for the effective range of stress intensity factor throughout the growth rate transients that accompany the overload cycle. This allows identification of how well the observed crack growth rate change can be correlated with plasticity-induced shielding. The experimental work uses the CJP elastic crack tip field model [1] to predict the evolution in size and shape of the crack tip plastic zone before, during and immediately after, the application of single spike overloads of 20% and 50%. The CJP predictions of plastic zone size and shape were verified using an experimental DIC methodology developed by Vasco-Olmo et al [2] that is also based on crack tip displacement fields.

The work reported in this paper is the first time that an elastic crack tip field model has been used to obtain accurate predictions of both the effective range of stress intensity factor and the changes in plastic zone size and shape that occur during variable amplitude fatigue, and to then assess how well the changes in crack growth rate can be correlated with the effects of plasticity-

induced shielding. The conclusions from the research therefore inform a better understanding and more accurate assessment of fatigue crack growth transients during variable amplitude loading and the role of plasticity-induced shielding.

2. Outline of the CJP model of crack tip fields

In the literature there are several models that describe crack tip stress or displacement fields. A previous work by some of the present authors [2] explored the capability of three different elastic crack tip field models (Westergaard [19], Williams [20], [21] and CJP [12]) to predict the size and shape of the crack tip plastic zone. The results obtained in that work led to the conclusion that the CJP model provided the most accurate predictions of plastic zone size and shape when compared to experimental data. This is perhaps not surprising as the CJP model was specifically developed as an endeavour to obtain an elastic stress field model that explicitly captures the influences on the applied elastic stress field of an embedded region of plasticity surrounding a growing fatigue crack. It is believed that it provides a better characterisation of that forces and stresses that arise from the plastic enclave surrounding a crack and that lead to plasticity-induced shielding. The model has been developed and solved in terms of both stress and displacement fields around the crack tip and therefore can be directly calibrated against full field phase-stepping photoelasticity [22] or against DIC [12].

The present paper extends the previous work on plastic zone size and shape to the consideration of the influence of plasticity-induced shielding during fatigue overload cycles. Hence the CJP model is applied to the prediction of plastic zone shape and size under variable amplitude loading, as the stress intensity factors defined in the CJP model explicitly account for plasticity-induced shielding during fatigue crack growth [12]. Thus plastic zone development, effective stress intensity factor and crack growth rate can be followed (on a cycle-by-cycle basis) throughout the period affected by the overload. It is then possible to examine the possibility of any direct correlation between plasticity-induced shielding (evidenced as changes in the effective ΔK value) and crack growth transients.

The CJP model is a model of the elastic crack tip fields developed by Christopher, James and Patterson [12] that is based on Muskhelishvili's complex potentials [23]. It defines two new primary stress intensity factors K_F and K_R. K_F is the stress intensity factor that drives crack growth and K_R is the stress intensity factor that acts to retard crack growth. The difference between the two stress intensity factors explicitly provides the effective crack driving force, $\Delta K_{eff} = (K_F - K_R)_{max} - (K_F - K_R)_{min}$. The model considers that the plastic enclave surrounding a fatigue crack acts to shield it from the full influence of the elastic stress field that drives the fatigue crack growth and that these plasticity-induced effects can be assessed from consideration of the elastic field.

The innovative postulate in the model is that the mathematical formulation of this crack tip shielding includes not only a contribution from the effect of crack flank contact forces (so-called crack closure) that exponentially decays behind the crack tip, but also compatibility-induced stresses at the elastic-plastic boundary. James et al [24],[12] have previously provided a schematic idealisation of the crack tip forces postulated to be acting at the interface between the plastic zone and the surrounding elastic material. The underlying concept in the model is that plastic zone influences on crack growth will be captured, in terms of crack growth effects, by net elastic contributions acting at the elastic–plastic boundary.

The CJP characterisation of the elastic stress field has been given in reference 2 and five coefficients (A', B', C', E' and F') are needed to define its components around the crack tip. In addition, this mathematical description of the crack tip stress fields assumes that the origin of the coordinate system is located at the crack tip; in the Cartesian coordinate system they are defined parallel with, and perpendicular to, the current crack direction. In polar coordinates, the $\theta = 0$ direction is defined along the current crack growth direction. In a similar way, the displacement field around the crack tip was presented in reference 12.

In the mathematical analysis of either stress or displacement, the assumption $D' + E' = 0$ is made in order to give an appropriate asymptotic behaviour of the wake contact stress along the crack flank. The CJP model of stress and displacement fields around the crack tip therefore has

four independent parameters. These are associated with the stress intensity factor K_F that drives crack growth, the retardation stress intensity factor K_R, a shear stress intensity factor K_S and the T-stress T. The authors have not yet identified whether the term K_S serves a useful role in Mode I fatigue crack growth, but significant evidence indicates that the effective stress intensity range in Mode 1 fatigue crack growth is accurately predicted by the difference between K_F and K_R, e.g. [25].

K_F is defined using the applied remote load usually used to characterise K_I but which is modified by force components derived from the stresses acting across the elastic-plastic boundary (that, in turn, arise from wake contact and strain compatibility) and which therefore influence the driving force for crack growth. K_F is defined from the asymptotic limit of σ_y as $x \rightarrow +0$, along $y = 0$, i.e. towards the crack tip on the crack plane ahead of the crack tip:

$$K_F = \lim_{r\to 0}\left[\sqrt{2\pi r}\left(\sigma_y + 2E' r^{-\frac{1}{2}} \ln r\right)\right] = \sqrt{\frac{\pi}{2}}\left(A' - 3B' - 8E'\right) \tag{1}$$

When there is no plasticity-induced shielding $K_F = K_I$ and the difference between the two parameters increases as the magnitude of the shielding effect gets larger. K_R characterises forces arising from compatibility and plasticity-induced shielding and that act in the plane of the crack and whose effect is experienced ahead of the crack tip. They provide a direct retarding effect on fatigue crack growth. K_R is evaluated from σ_x in the limit as $x \rightarrow -0$, along $y = 0$, i.e. towards the crack tip from behind along the crack flank:

$$K_R = \lim_{r\to 0}\left[\sqrt{2\pi r}\,\sigma_x\right] = -(2\pi)^{\frac{1}{2}} E' \tag{2}$$

The T-stress, which is found as components T_x in the x-direction and T_y in the y-direction is given by:

$$\begin{aligned} T_x &= -C' \\ T_y &= -F' \end{aligned} \tag{3}$$

3. Experimental work

The experimental work was performed on two Grade 2 commercially pure titanium CT specimens with different dimensions, as given in Figure 1. These wo different sizes of specimen were chosen to test whether the model would give sensible and comparable data over a range of sizes and geometries – future work will incorporate results from edge-notched and centre-cracked tension specimens. The overload fatigue test parameters are defined in Table 1, where constant amplitude loading formed the baseline case with single spike overloads being applied once the crack was growing in a stable fashion well outside the original notch plastic zone. The values of K_{max} and ΔK given in Table 1 are the standard Irwin values for the CT specimen. Where a repeat overload was applied, the crack was grown a distance of at least two times the overload monotonic plastic zone size before the second overload was applied. Tables 2 and 3 respectively present the chemical analysis and mechanical property data for the CP titanium alloy used in the work. Grade 2 titanium has numerous applications in the medical industry because of its excellent biocompatibility, and in marine and high temperature applications involving aqueous environments because of its high corrosion resistance.

Specimens were prepared for the experimental DIC and crack length measurements in the following manner. The surface used for the DIC work was sprayed with a black speckle pattern over a white background using a small airbrush, while the other face of the specimen was polished to assist in tracking the crack tip and measuring the crack length with a zoom lens.

An ElectroPuls E3000 dynamic testing machine (Figure 2) was used for fatigue testing. Constant amplitude loading at a frequency of 10 Hz and stress ratios of either R = 0.1 and 0.6 were applied to the two CT specimens. A CCD camera fitted with a macro-zoom lens (MLH-10X EO) was placed perpendicular to each face of the specimens to provide the necessary spatial resolution in the measurement region surrounding the crack tip. The field of view was 17.3 mm by 13 mm (giving a spatial resolution of 13.5 μm/pixel) for specimen CT1 and 13.1 mm by 9.7 mm (giving a spatial resolution of 8.07 μm/pixel) for specimen CT2. During fatigue testing, a sequence of images was captured at different load levels through complete loading and unloading cycles; this involved periodically pausing the fatigue cycling and applying stepwise

loading through a fatigue cycle making measurements at each step. The crack path was located to be at the centre of the image and the speckled surface of the specimens was illuminated with a fibre optic ring placed around the zoom lens (also shown in Figure 2).

4. Experimental methodology for the plastic zone quantification

Although the methods used for plastic zone quantification have been described in detail in reference 2, the method is sufficiently novel that it is worth providing an outline in the present paper of the two DIC techniques used to evaluate the size and shape of the crack tip plastic zone. The first method uses the CJP model of crack tip stress and displacement fields to predict plastic zone size and shape while the second method gives a direct estimation of the size and shape from differentiation of the experimentally measured crack tip displacement fields. The close correlation observed between the results obtained with the two methods provides confidence that the CJP values of effective stress intensity range accurately reflect the plasticity-induced shielding arising from both crack wake contact and the compatibility requirements between the embedded plastic zone and the surrounding elastic material.

4.1. Experimental method for estimating the plastic zone

The von Mises yield criterion is used to determine plastic zone size and shape by substituting the uniaxial tensile stress into the equation for the equivalent yield stress as a function of polar angle around the crack tip. The equivalent yield stress expression is obtained from analysing the experimentally measured displacement field. The various steps followed in implementing this methodology are shown in Figure 3. The first step consists in obtaining the horizontal and vertical displacement fields around the crack tip, using a two dimensional DIC technique. Figure 4 shows typical examples of the horizontal and vertical displacement maps (resolution of 14.8 pixel/mm) obtained for specimen CT1 at a crack length of 8.27 mm and a load of 750 N. All the steps in the process will be illustrated using these displacement maps. The next step involves determining the strain field at the crack tip by differentiating the displacement field. Differentiation was performed every two pixels and the Green-Lagrange strain tensor [26] was employed for this, since it also considers second order nonlinear terms that provide a more

accurate description of high deformation fields than can be obtained using only first-order terms. Thus the strain tensor is given by the following expression:

$$\begin{pmatrix} \varepsilon_{xx} \\ \varepsilon_{yy} \\ \varepsilon_{xy} \end{pmatrix} = \begin{pmatrix} \frac{\partial u}{\partial x} \\ \frac{\partial v}{\partial y} \\ \frac{\partial u}{\partial y} + \frac{\partial v}{\partial x} \end{pmatrix} + \frac{1}{2} \begin{pmatrix} \frac{\partial u}{\partial x} & 0 & \frac{\partial v}{\partial y} & 0 \\ 0 & \frac{\partial u}{\partial y} & 0 & \frac{\partial v}{\partial y} \\ \frac{\partial u}{\partial y} & \frac{\partial u}{\partial x} & \frac{\partial v}{\partial y} & \frac{\partial v}{\partial x} \end{pmatrix} \begin{pmatrix} \frac{\partial u}{\partial x} \\ \frac{\partial u}{\partial y} \\ \frac{\partial v}{\partial x} \\ \frac{\partial v}{\partial y} \end{pmatrix} \tag{4}$$

Figure 5 shows the strain maps (ε_{xx}, ε_{yy} and ε_{xy}) obtained from the displacement field shown in Figure 4. Once the strain field has been calculated, the next step is to calculate the stress field (σ_{xx}, σ_{yy} and σ_{xy}) using Hooke's law:

$$\begin{aligned} \sigma_{xx} &= \frac{E}{1-\nu^2}\left(\varepsilon_{xx} + \nu\varepsilon_{yy}\right) \\ \sigma_{yy} &= \frac{E}{1-\nu^2}\left(\varepsilon_{yy} + \nu\varepsilon_{xx}\right) \\ \sigma_{xy} &= \frac{E}{1+\nu}\varepsilon_{xy} \end{aligned} \tag{5}$$

Figure 6 shows the stress maps (σ_{xx}, σ_{yy} and σ_{xy}) calculated from the strain maps shown in Figure 5. The equivalent stress is then calculated from the stress tensor via a yield criterion. In a previous paper [2], both the von Mises and the Tresca yield criteria were used to estimate the position where the equivalent stress was higher than the yield limit of the material, as a function of the polar angle around the crack tip. This then provides both size and shape of the plastic zone. As expected, the size obtained using the Tresca criterion was slightly larger than that found using the von Mises criterion, but close agreement was observed in both cases between the experimentally determined plastic zone and the predictions of the CJP model.

The von Mises criterion is used in the present work as it has been widely applied to modelling plastic deformation in α-titanium in situations where the strain rates are relatively low and deformation twinning is limited. Figure 7a is an image of the von Mises equivalent stress map obtained for specimen CT1 at a crack length of 8.27 mm and a load level of 750 N. The size and shape of the plastic zone is estimated by identifying the region where the yield criterion is met,

i.e., where the equivalent stress is equal to the yield stress and Figure 7b shows this plastic region. Thus, the plastic zone area (white) can easily be identified from the surrounding elastic field.

In this paper, the area of the plastic zone is considered as a variable that contains information on both size and shape and which can therefore provide an efficient and powerful tool for making quantitative measurements. To quantify its area at the crack tip a set of data points must be identified that define the equivalent yield stress contour of the plastic zone. Next, a triangulation technique is applied to define the area enclosed by this contour. Finally, the plastic zone area can be calculated as the sum of the areas for all the triangles defined in the triangulation process.

4.2. Indirect method for estimating the plastic zone

The two most widely used methods in the literature to estimate plastic zone size are the Irwin and Dugdale approaches [27]. Both approaches are based on elastic stress field solutions and lead to simple estimates for crack tip plastic zone size. However, the plastic zone shape assumed in these models does not match that experimentally observed in metals [27]. A more useful technique is to estimate the extent and shape of the plastic zone as a function of angle around the crack tip by applying a yield criterion to an analytical model [12], [19], [20], [28] that describes the crack tip stress field.

The CJP model of stress and displacement fields around the crack tip is well suited to determining plastic zone size and shape as a function of angle as both fields are defined as a function of a set of coefficients (A', B', C', E', F') and polar coordinates (r, θ) of the data points around the crack tip. The first step in using the model to estimate plastic zone size and shape therefore requires determining the set of coefficients that the model uses, from analysis of the displacement fields obtained by DIC using a multi-point over-deterministic method as developed by Sanford and Dally [29]. The CJP model is valid only in the near-tip elastic field region and hence it is necessary to identify a suitable region surrounding the crack tip where valid experimental data can be obtained.

An annular mesh (Figure 8) was therefore defined with an inner radius large enough to avoid including plastic deformation at the crack tip and an outer radius that lies within the region dominated by the elastic stress singularity. The vertical displacement field can be used to identify this outer radius by observing changes in the field orientation that originate from the interaction between the singularity dominated region and that dominated by specimen edge effects. This limit is easily identified because the displacement field orientation becomes straight and perpendicular to the crack (see Figure 8). In addition, the accuracy of location of the crack tip position is important, and this was optimised through statistical assessment of the quality of the fit between the mathematical solution of the displacement field and the experimental data, using the mean and the variance. The crack tip position is regarded as that point that gives the lowest values of the mean and variance as a function of the crack tip coordinates. The region of plasticity along the crack flanks is also masked out from data collection.

Once coefficients in the CJP model have been determined, they can be used to calculate the crack tip stress field. This field is a function of the coefficients and the polar coordinates of the data points collected and the equivalent von Mises stress can therefore also be obtained as a function of these parameters. An error function can be then defined to represent the difference between the equivalent von Mises stress and the uniaxial yield stress of the material:

$$f_{error} = \sigma_{eq}\left(A', B', C', E', F', r, \theta\right) - \sigma_{ys} = 0 \tag{6}$$

Solving this function for all angles $0° \leq \theta \leq 360°$ defines the yield boundary contour which can then be used to obtain the required information on plastic zone size and shape. Figure 9 compares the experimentally determined plastic zone shape (white area) with the CJP prediction (yellow line) for the CT1 specimen with a crack length of 8.27 mm. There is clearly a high degree of correspondence between the two results.

5. Results and discussion

5.1. Plastic zone evolution during and after an overload

Figure 10 shows the data obtained for plastic zone size and shape at the maximum applied stress amplitude before, during, and immediately after the application of either 20% or 50% overloads at crack lengths between 6.19 mm and 17.12 mm (see Table 1). In all cases, there is a good agreement between the experimental data and the predictions of the CJP model. Figures 10a, 10b and 10c compare the plastic zone size and shape obtained immediately prior to the overload, during the overload itself, and during the first post-overload fatigue cycle, for the case of a 50% overload applied at a crack length of 6.19 mm on specimen CT1 (undergoing constant amplitude loading at R = 0.6). The data obtained for overloads of amplitude 20% and 50% on specimen CT2 experiencing constant amplitude loading at R = 0.1 are shown in Figures 10d to 10f and 10g to 10i respectively.

Each overload produced a large increase in area of the crack tip plastic zone during the overload cycle and left a residual increase even after the applied load returned to the pre-overload level. Table 4 presents the data for plastic zone area for both specimens. For CT2 (constant amplitude loading at R = 0.1) a 170% increase in experimentally measured plastic zone area occurred during the overload cycle and the plastic zone was still 25.8% bigger in the load cycle immediately subsequent to the overload. For a 50% overload on CT2 the equivalent figures are 134% and 40.4%, whilst for a 50% overload on CT1 (constant amplitude loading at R = 0.6) the figures are 342% during the overload cycle and 43.4%.

The relative sizes of plastic zone measured during the overload cycles in the three cases are both interesting and difficult to easily explain. The lower level of reversed plasticity that would occur during cycling at R = 0.6 compared with R = 0.1, would influence the local hardening/softening behaviour. Handfield and Dickson [30] in their work on the cyclic deformation of annealed CP titanium (equivalent to Grade 2) note that the room temperature cyclic behaviour for material initially in the annealed state shows for reversed total strain amplitudes between ±0.15% and 0.75%, initial cyclic hardening followed by cyclic softening. For material prestrained in tension, they found that the relaxation of the residual stress influenced cyclic effects.

Consider, for example, the data for the 50% overloads where the K_{max} value in both cases (R = 0.1 and 0.6) is the same both before and during the overload, while the range of stress intensity factor is very different. The difference in shape and area between the plastic zones corresponding with the two cases is interpreted as demonstrating that plasticity is influenced both by K_{max} and ΔK in the fatigue cycle. Whilst this might seem an obvious conclusion, the less obvious aspect is the relative contribution that each parameter in the fatigue cycling makes to the shape and area. It is believed that the techniques outlined in the present paper offer a new way to explore these influences and, in combination with accurate prediction of the effective driving force for crack growth, will yield new insights into plasticity-induced shielding of growing fatigue cracks subject to variable amplitude loading.

The data obtained during the load cycle immediately after the overload follows a more predictable trend, being approximately 26% larger after a 20% overload and approximately 41-43% larger after a 50% overload irrespective of whether the stress ratio is 0.1 or 0.6.

One point that is noticeable in Figure 10, particularly in the images from CT2 subsequent to the second overload, is an asymmetry across the plane of the crack in the plastic zone shape, the reason for this is not known, but it is possible that it reflects ratcheting, which is known to occurs in CP titanium [31]. It is clear that the effect of crack plasticity on crack growth rate during an overload may reflect influences from shielding, ratcheting and K_{max}.

The change in size of plastic zone can be tracked as the crack grows through the overload plastic zone. Figure 11 shows such data and compares the experimental and predicted plastic zone areas (A_{PZ}) as a function of crack length for both CT specimens. In all cases, the experimental data is in close agreement with the predictions obtained with the CJP model. Prior to the overload, the plastic zone area increases steadily with crack length, with the application of the overload giving a significant immediate increase in plastic zone area. In the loading cycle immediately following the overload, the plastic zone area decreases significantly but remains larger than the pre-overload value. During continued post-overload fatigue cycling, a gradual decrease in the plastic zone area is observed towards the pre-overload trend in the data. The

decay in plastic zone area is sustained longer in the case of a 50% overload. Vertical lines have been added to Figure 11a and 11b indicating the influence zone of each overload. The influence of a 50% overload extends over 0.21 mm, equivalent to 1900 load cycles, for the CT1 specimen (R = 0.6). In the case of the CT2 specimen (R = 0.1), the influence of the 20% overload extends over 0.26 mm (610 cycles), while that of the 50% overload extends over 0.51 mm (1600 cycles).

The evolution of plastic zone size and shape with crack growth through the overload region can also be easily visualised by plotting sequential CJP model predictions for the CT1 specimen. Figure 12 presents three illustrations of this shape evolution, giving two different 2D views and a 3D depiction. Figure 12a presents a fairly typical illustration of the usual bean-shaped plastic zone in Grade 2 titanium, while Figure 12b presents a line illustration showing maximum size in the vertical y-direction. The 3D view given in Figure 12c provides perhaps the clearest illustration of plastic zone development. In all three cases, the overload position during crack growth is clearly seen in the clustering of the data and in Figures 12b and 12c, by the localised increase in size.

5.2. Crack growth rate and effective stress intensity factor range

The period of growth over which this gradual decrease in plastic zone area is observed following the overload cycle is associated with a retardation effect on fatigue crack growth as the crack propagates through the enlarged plastic zone generated by the overload [16]–[18]. This retardation is evidenced in the crack growth rate trends. Figure 13 presents a graph of fatigue crack growth rate (da/dN) versus both the nominal (Irwin) and the effective (CJP) stress intensity factor range (ΔK_{eff}) for the CT1 specimen (50% overload). ΔK_{eff} has been calculated as the difference between the K_F and K_R values at maximum and minimum load as indicated in section 2, i.e. $\Delta K_{eff} = (K_F - K_R)_{max} - (K_F - K_R)_{min}$. The nominal stress intensity factor range (defined using the standard Irwin stress intensity values, i.e. $\Delta K_{nom} = K_{max} - K_{min}$) after the application of the overload has been also plotted in Figure 13. A period of constant amplitude crack growth is shown between points 1 and 2 in which the values increase as expected based

on the Paris law. When the overload is applied there is a brief acceleration in the crack growth rate to point 3 which is followed by a substantial decrease in both crack growth rate and effective stress intensity factor range (point 4). Note that the nominal stress intensity value has the same value after the overload that it had before, while the effective value given by the CJP model shows a significant decrease. A gradual increase in the crack growth rate is subsequently observed until point 5, with the retardation of fatigue crack growth during this period being a result of the plasticity induced by the applied overload. From point 5 onwards, fatigue crack growth rates resume the trend observed prior to the application of the overload. Figure 14 shows the predicted trends in the CJP stress intensity parameters K_F and K_R plotted against crack length. Table 4 gives the relevant values of K_F and K_R for the two CT specimens before the overload, during the overload and immediately after the overload.

Figure 15 plots the effective stress intensity range that is predicted by the CJP model, and compares the data with the nominal ΔK value. The reduction of ΔK_{eff} following the application of a 50% overload can be clearly observed and related to the changes in crack growth rates. Figure 13 shows that plotting growth rate data against the effective stress intensity factor derived from the CJP model does not eliminate the immediate acceleration and subsequent retardation associated with an overload. As mentioned above, the changes in shape and size of the plastic zone observed in this work indicate that the effect of crack plasticity on crack growth rate during, and subsequent to, an overload may reflect influences from shielding (evidenced through the reduction observed in the CJP value of ΔK_{eff}), ratcheting and K_{max}. Several authors have previously proposed that the effect of stress ratio on crack growth rate is better rationalised by a two parameter approach using ΔK and K_{max}, e.g. [32]. Further work exploring a potential two-parameter characterisation of stress intensity factor during overloads as a function of stress ratio is currently planned.

6. Conclusions

The work reported in the present paper on compact tension specimens manufactured from a commercially pure Grade 2 titanium sheet with a thickness of 1 mm has quantitatively

compared experimentally determined plastic zone size, shape and area data [2] with predictions obtained from the CJP model of crack tip stress and displacement before, during and after 20% and 50% overloads. The experimental methods used differentiation of the displacement fields measured by DIC to obtain strain maps that can be combined with a yield criterion to estimate the shape and size of the crack tip plastic zone. The results obtained from the CJP model [12] showed a very good level of agreement with the experimental data, and demonstrate that the model is a powerful tool in accurate characterisation of the size, shape and area of the crack tip plastic zone, through its original formulation that incorporates the likely influences of crack tip and crack wake plasticity on the elastic stress fields ahead of the crack.

The fatigue crack growth rate data show the expected retardation effect following either a 20% or a 50% overload, with the period of retardation being longer in the case of the 50% overloads. A comparison of overloads applied with the same nominal K_{max} values at stress ratios of 0.1 and 0.6 has demonstrated that the size and shape of the plastic zone is influenced both by K_{max} and ΔK in the fatigue cycling.

This work presented in this paper reinforces the view presented in previous papers that the CJP model provides a very useful tool for the study of fracture mechanics problems such as plasticity-induced crack shielding [13], the retardation effect induced by overloads on fatigue crack growth [33] and the mechanisms that may play a role in the crack growth retardation.

Importantly, this work has also demonstrated that plasticity-induced shielding is not a complete explanation for the observed crack growth rate changes during and after an overload. The observed changes in shape and size of the plastic zone indicate that the effect of crack plasticity on crack growth rate during, and subsequent to, an overload may reflect influences from shielding (evidenced through the reduction observed in the CJP value of ΔK_{eff}), ratcheting and K_{max}.

Acknowledgements

The current work has been conducted with financial support from Gobierno de España through the project 'Proyecto de Investigación de Excelencia del Ministerio de Economía y Competitividad MAT2016-76951-C2-1-P' and financial support for Bing Yang from the Chinese Scholarship Council. These contributions are gratefully acknowledged.

References

[1] Christopher CJ, James MN, Patterson, EA and Tee KF (2007). Towards a new model of crack tip stress fields. Int. J. Fract., 148, 361-371.

[2] Vasco-Olmo JM, James MN, Christopher CJ, Patterson EA and Díaz FA (2016). Assessment of crack tip plastic zone size and shape and its influence on crack tip shielding. Fatigue Fract. Engng Mater Struct., 39, 969-981.

[3] Nowell, D. Dragnevski, KI and O'Connor, SJ (2018). Investigation of fatigue crack models by micro-scale measurement of crack tip deformation, Int. J. Fatigue, in press.

[4] Uğuz A and Martin JW (1996). Plastic zone size measurement techniques for metallic materials, Materials Characterization, 37, 105-118.

[5] James MN, Hattingh DG, Hughes DJ, Patterson EA and Quinta da Fonseca J (2004). Synchrotron diffraction investigation of the distribution and influence of residual stresses in fatigue. Fatigue Fract. Engng Mater. Struct., 27, 609-622.

[6] Steuwer A, Edwards L, Pratihar S, Ganguly S, Peel M, Fitzpatrick ME, Marrow TJ, Withers PJ, Sinclair I, Singh KD, Gao N, Buslaps T and Buffière JY (2006). In situ analysis of cracks in structural materials using synchrotron X-ray tomography and diffraction, Nuclear Instruments and Methods in Physics Research Section B: Beam Interactions with Materials and Atoms, 246, 217-225.

[7] Zhang W and Liu Y (2011). Plastic zone size estimation under cyclic loadings using in situ optical microscopy fatigue testing. Fatigue Fract. Engng Mater. Struct., 34(9), 717-727.

[8] Patki AS and Patterson EA (2010). Thermoelastic stress analysis of fatgiue cracks subject to overloads. Fatigue Fract. Engng Mater. Struct., 33, 809-821.

[9] Wright SI, Nowell MM, Field DP (2011). A review of strain analysis using electron backscattter diffraction. Microscopy and Microanalysis, 17, 316-329.

[10] Yang Y, Crimp M, Tomlinson RA and Patterson EA (2012). Quantitative measurement of plastic strain field at a fatigue crack tip. Proc. R. Soc. A, 468, 2399-2415.

[11] Carroll JD, Abuzaid W, Lambros J and Sehitoglu H (2013). High resolution digital image correlation measurements of strain accumulation in fatigue crack growth. Int. J. Fatigue, 57, 140-150.

[12] James MN, Christopher CJ, Lu Y and Patterson EA (2013). Local crack plasticity and its influences on the global elastic stress field. Int. J. Fatigue, 46, 4-15.

[13] Vasco-Olmo JM, Díaz FA, García-Collado A and Dorado R (2015). Experimental evaluation of crack shielding during fatigue crack growth using digital image correlation. Fatigue Fract. Engng Mater. Struct., 38, 223-237.

[14] James MN (1997). Some unresolved issues with fatigue crack closure - measurement, mechanism and interpretation problems, Advances in Fracture Research, Proceedings of the Ninth International Conference on Fracture, Sydney, (eds. B L Karihaloo et al), Australia, April 1997, Pergamon Press, 5, 2403-2414.

[15] Wei RP and Shih TT (1974). Delay in fatigue crack growth. Int. J. Fract., 10, 77-85.

[16] Corbly DM and Packman PF (1973). On the influence of single and multiple peak overloads on fatigue crack propagation in 7075-T6511 aluuminium. Eng. Fract. Mech., 5, 479-497.

[17] Shin CS, Hsu and SH (1993). On the mechanisms and behaviour of overload retardation in AISI-304 stainless steel. Int. J. Fatigue, 15, 181-192.

[18] Sadananda K, Vadusevan AK, Holtz RL and Lee EU (1999). Analysis of overload effects and the related phenomena. Int. J. Fatigue, 21, S233-S246.

[19] Janssen M, Zuidema J and Wanhill RJH (2006). *Fracture Mechanics*. Spon Press, Abingdon, UK.

[20] Ramesh K, Gupta S and Kelkar AA (1997). Evaluation of stress field parameters in fracture mechanics by photoelasticity—Revisited. Eng. Fract. Mech., 56, 25-45.

[21] Yates JR, Zanganeh M and Tai YH (2010). Quantifying crack tip displacement fields with DIC. Eng. Fract. Mech., 77, 2063-2076.

[22] Pacey MN, Patterson EA and James MN (2005). A new photoelastic model for studying fatigue crack closure, Experimental Mechanics, 45, 42-52.

[23] Muskhelishvili NI (1977). *Some Basic Problems of the Mathematical Theory of Elasticity*. Noordhoff International Publishing, Groningen, The Netherlands.

[24] Christopher CJ, James MN, Patterson EA, Tee KF (2008). A quantitative evaluation of fatigue crack shielding forces using photoelasticity. Eng. Fract. Mech., 75, 4190-4199.

[25] James MN, Christopher CJ, Díaz FA, Vasco-Olmo JM, Kakiuchi T and Patterson EA (2017), Interpretation of plasticity effects using the CJP crack tip field model, Solid State Phenomena, 258, 117-124.

[26] Singh AK (2010). *Mechanis of Solids*. Prentice-Hall of India, New Delhi, India.

[27] Anderson TL (2005). *Fracture Mechanics: Fundamentals and applications*. CRC Press LLC, Boca Raton, USA, 2005.

[28] Nurse AD, and Patterson EA (1993). Determination of predominantly mode II stress intensity factors from isochromatic data. Fatigue Fract. Engng Mater. Struct., 16, 1339-1354.

[29] Sanford RJ and Dally JW (1979). A general method for determining mixed-mode stress intensity factors from isochromatic fringe patterns. Eng. Fract. Mech., 11, 621-633.

[30] Handfield L and Dickson JI (1983) The Cyclic Deformation of Titanium: Dislocation Substructures and Effective and Internal Stresses. In: Sih G.C., Provan J.W. (eds) Defects, Fracture and Fatigue. Springer, Dordrecht.

[31] Ghosh A and Gurao NP (2017), Effect of chrystalographic texture on ratcheting response of commercially pure titanium. Mats and Design, 115, 121-132.

[32] James MN and Wenfing Li (1999), Fatigue crack growth in austempered ductile and grey cast irons–stress ratio effects in air and mine water. Mater. Sci. Engng, A265, 129-139.

[33] Vasco-Olmo JM and Díaz FA (2016). Experimental evaluation of the effect of overloads on fatigue crack growth by analysing crack tip displacemenet fields. Eng. Fract. Mech., 166, 82-96.

Tables

Table 1. Experimental test conditions for the fatigue tests.

Specimen reference	Loading conditions				Ratio R	Overload conditions				
	P_{min} (N)	P_{max} (N)	K_{max} (MPa·m$^{1/2}$)	ΔK (MPa·m$^{1/2}$)		%	P_{OL} (N)	a_{OL} (mm)	a/W	N_{OL} (cycles)
CT1	450	750	19.3	7.7	0.6	50	1125	6.19	0.31	77000
CT2	120	1200	19.3	17.3	0.1	20	1440	15.86	0.27	20700
						50	1800	17.12	0.30	23812

Table 2. Chemical composition of the commercially pure titanium Grade 2.

Element	Nitrogen	Carbon	Hydrogen	Iron	Oxygen	Titanium
Spec. wt%	≤0.05	≤0.08	≤0.015	<0.20	≤0.20	balance
Actual wt%	<0.01	0.01	0.002	0.10	0.12	balance

Table 3. Mechanical properties for the commercially pure Grade 2 titanium used in this work.

Mechanical property	**Unit**	**Value**
Young's modulus	MPa	105000
Yield stress	MPa	390
Ultimate stress	MPa	448
Elongation	%	20
Poisson's ratio	-	0.33

Table 4. Values of the plastic zone area and K_F and K_R values associated with 20% and 50% overloads.

Specimen	CT1		CT2			
% OL	50		20		50	
Area (mm^2)	Experimental	Predicted by CJP model	Experimental	Predicted by CJP model	Experimental	Predicted by CJP model
Before OL	1.4897	1.5548	2.1359	2.1803	3.1511	3.2249
During OL	6.5942	6.6376	5.7684	5.8412	7.3672	7.4812
After OL (% increase)	2.1379 (43.5)	2.2879 (47.1)	2.6870 (25.8)	2.7567 (26.4)	4.4237 (40.4)	4.4575 (38.2)
Specimen	CT1		CT2			
% OL	50		20		50	
SIFs (MPa·m$^{1/2}$)	K_F	K_R	K_F	K_R	K_F	K_R
Before OL	30.4281	0.0379	26.4771	0.5679	27.9325	0.4376
During OL	45.8936	-7.3328	32.0118	1.0267	42.0533	5.6521
After OL	30.3420	-0.0208	26.7742	0.3421	28.0706	0.6442

Figures

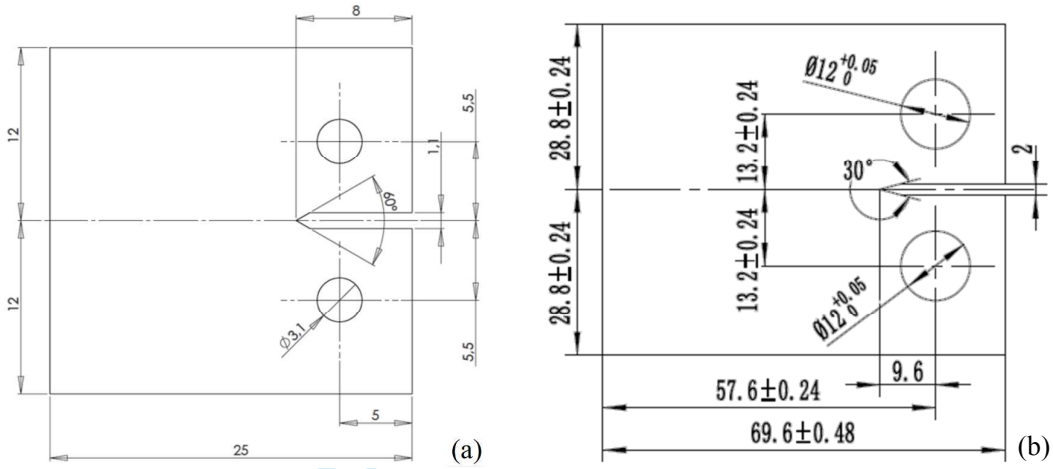

Figure 1 Geometry and dimensions (mm) of the titanium compact tension specimens used in this work. (a) CT1 specimen and (b) CT2 specimen.

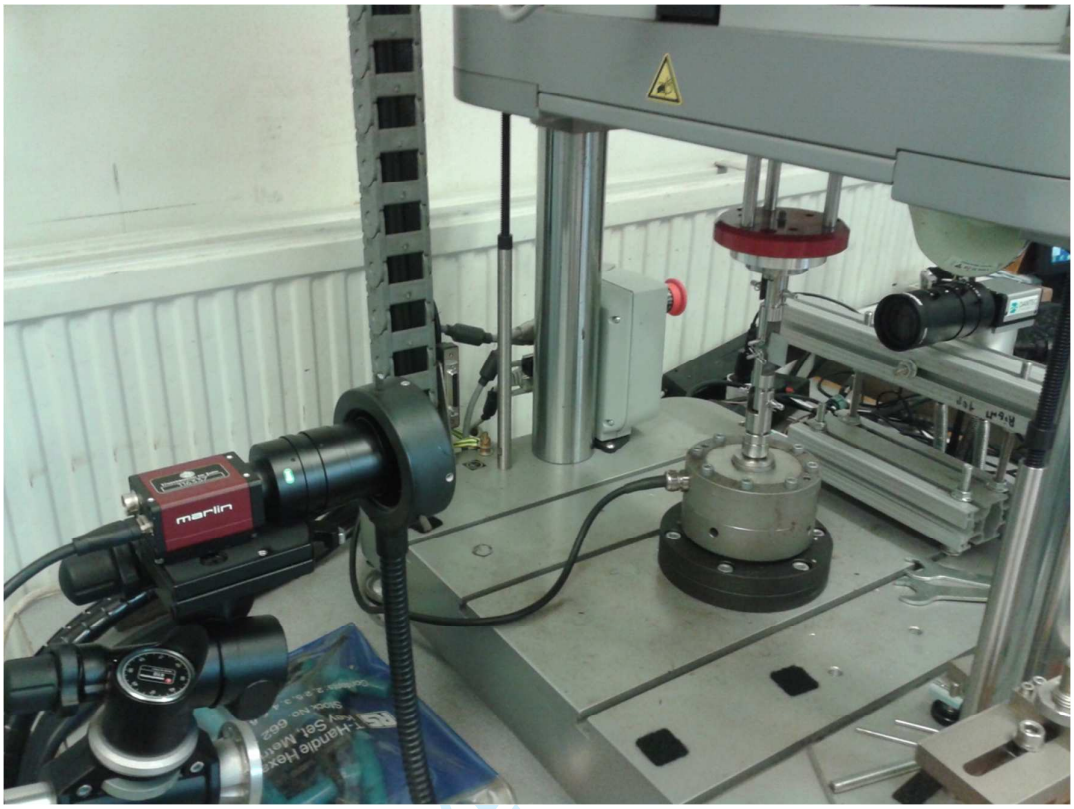

Figure 2 Experimental setup used to measure displacement fields by DIC and to track the crack tip during fatigue testing.

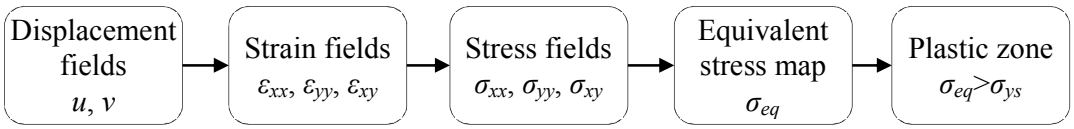

Figure 3 Block diagram of the process used in the direct estimation technique for estimating plastic zone area.

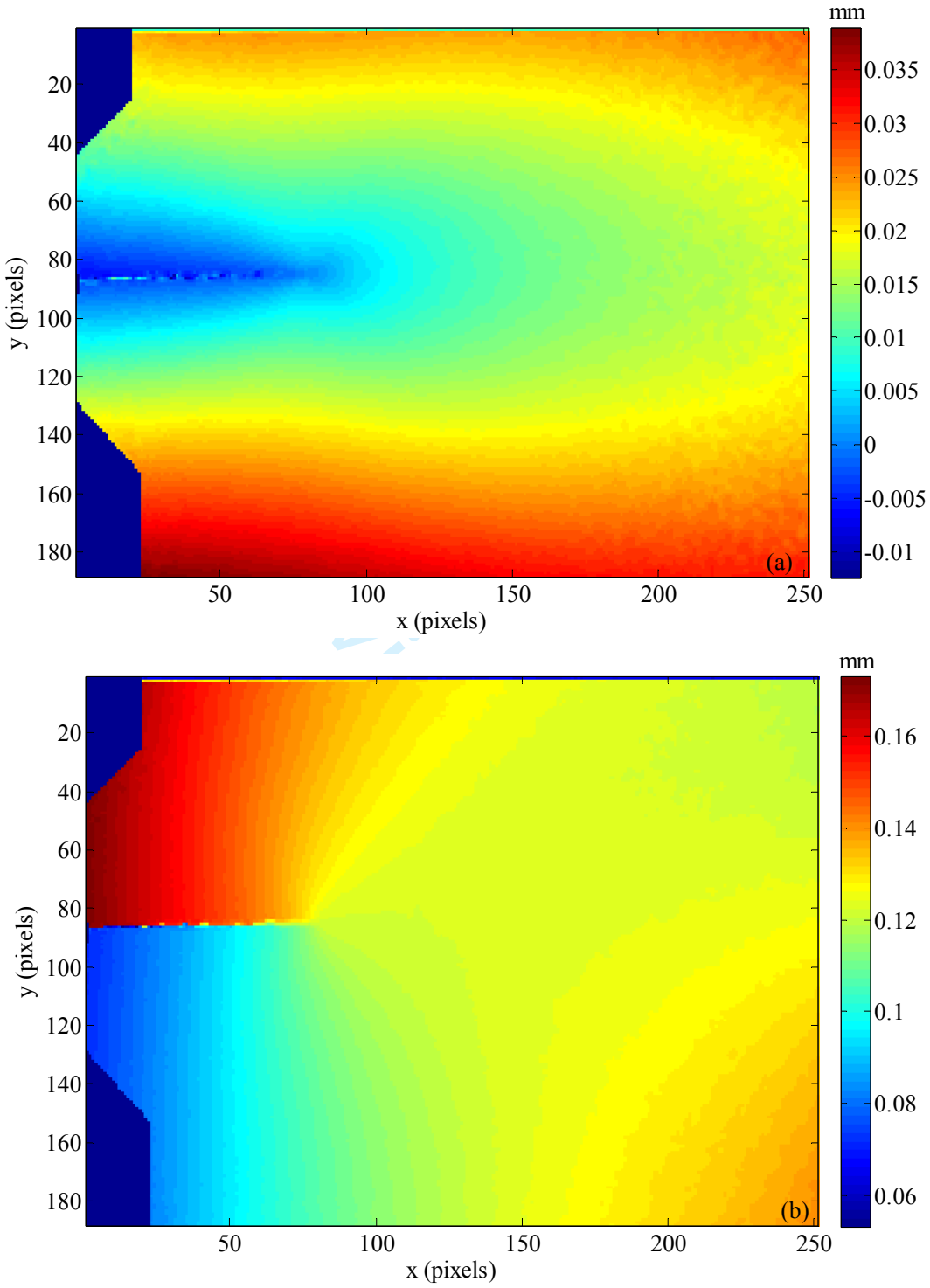

Figure 4 (a) Horizontal and (b) vertical displacement fields in the CT1 specimen measured by DIC for a crack length of 8.27 mm and a load level of 750 N.

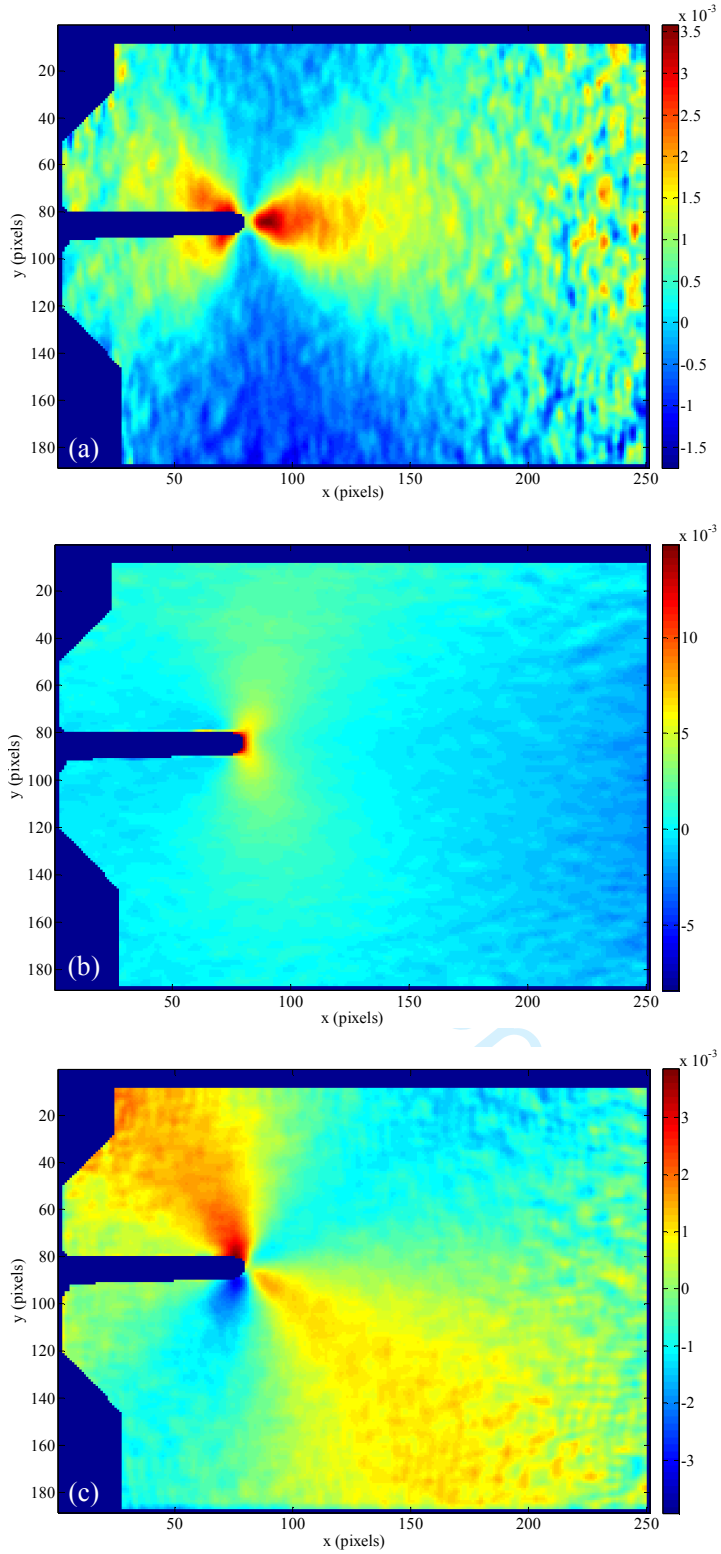

Figure 5 Strain maps for the CT2 specimen obtained by differentiating the displacement fields at a crack length of 8.27 mm and a load level of 750 N. (a) ε_{xx} (b), ε_{yy} and (c) ε_{xy}

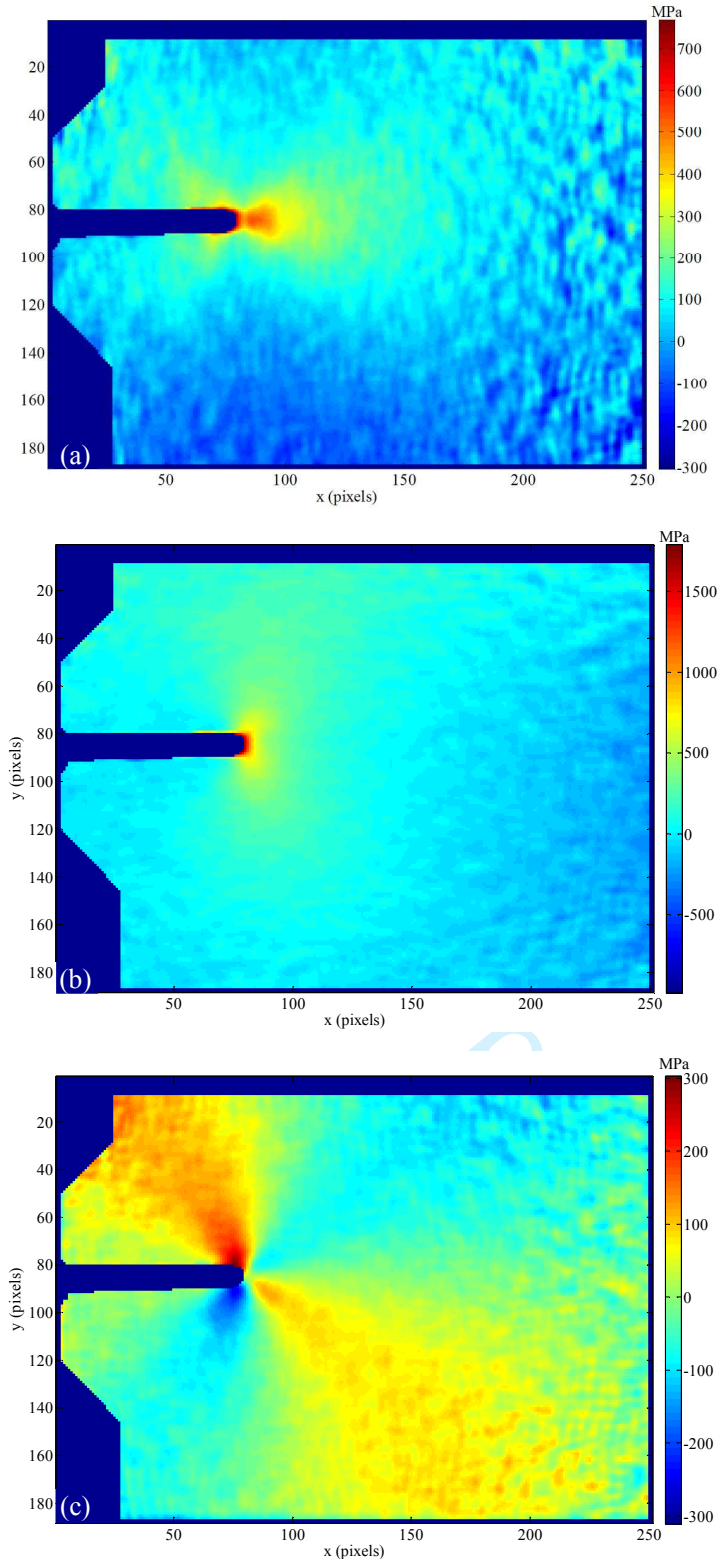

Figure 6 Stress maps for the CT1 specimen obtained from the strain fields at a crack length of 8.27 mm and a load level of 750 N. (a) σ_{xx} (b), σ_{yy} and (c) σ_{xy}

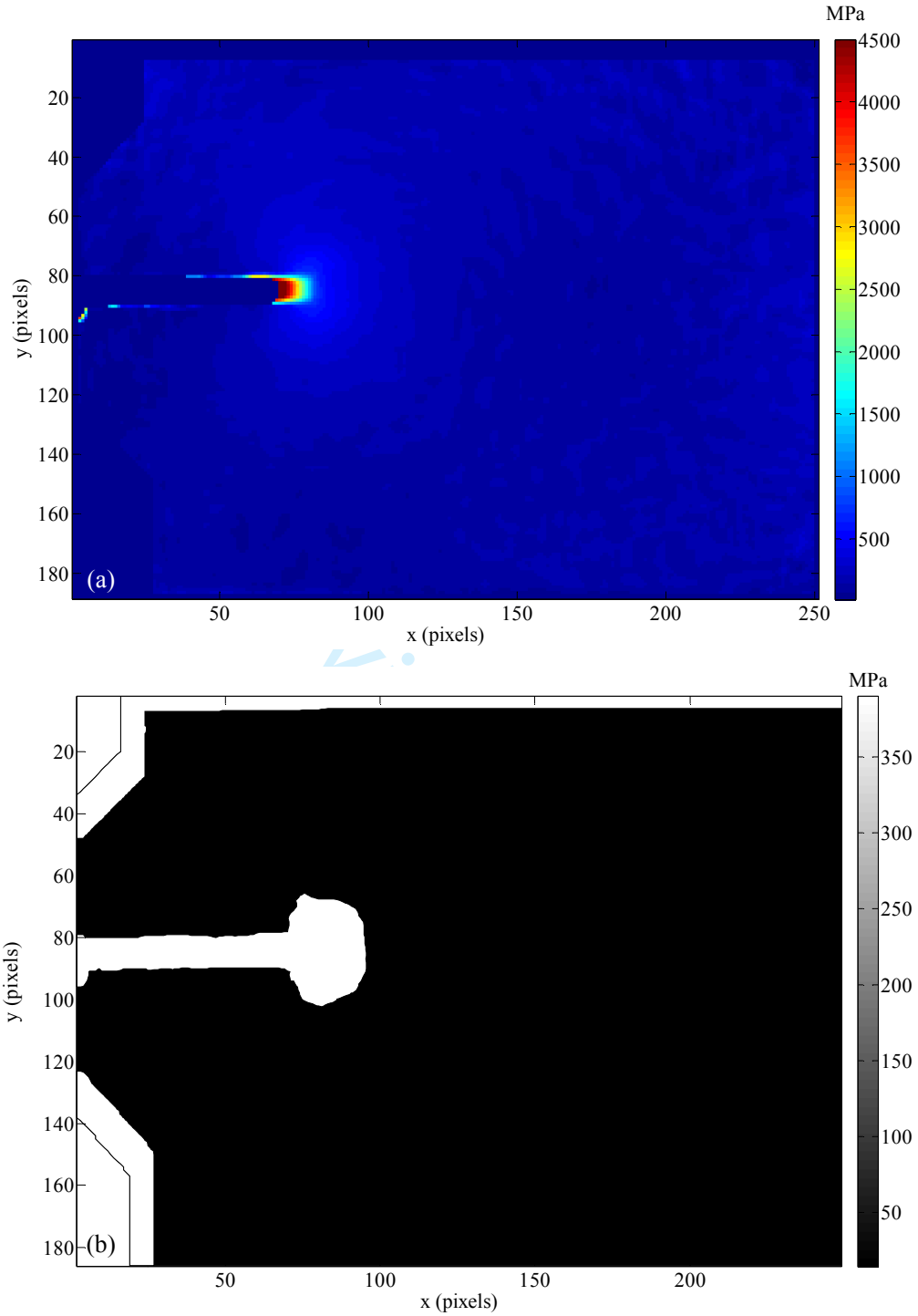

Figure 7 Illustrations of the von Mises equivalent stress map for a crack length of 8.27 mm in specimen CT1: (a) Directly obtained by implementing the method outlined in Figure 3 and (b) Processed to show the plastic zone around the crack tip as white region.

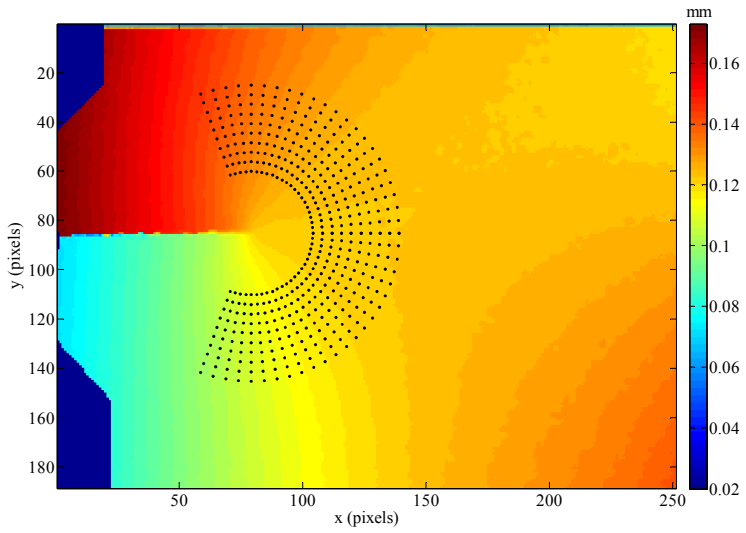

Figure 8 Annular mesh of data points used to define the appropriate near-tip region for the calculation of the CJP model coefficients. The change of orientation of the displacement field associated with the outer limit of valid data can be clearly seen in this figure, where the field orientation changes from turning back towards the crack tip to turning towards the back-face of the specimen.

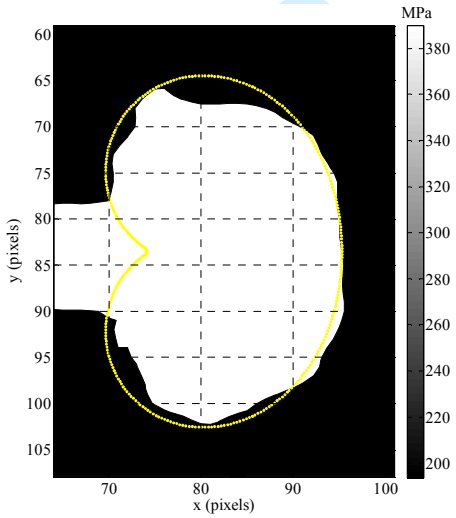

Figure 9 Illustration of the comparison between estimated plastic zones for the CT1 specimen at a crack length of 8.27 mm. The experimentally obtained plastic zone is the white region while the yellow contour line represents the plastic zone predicted by the CJP model.

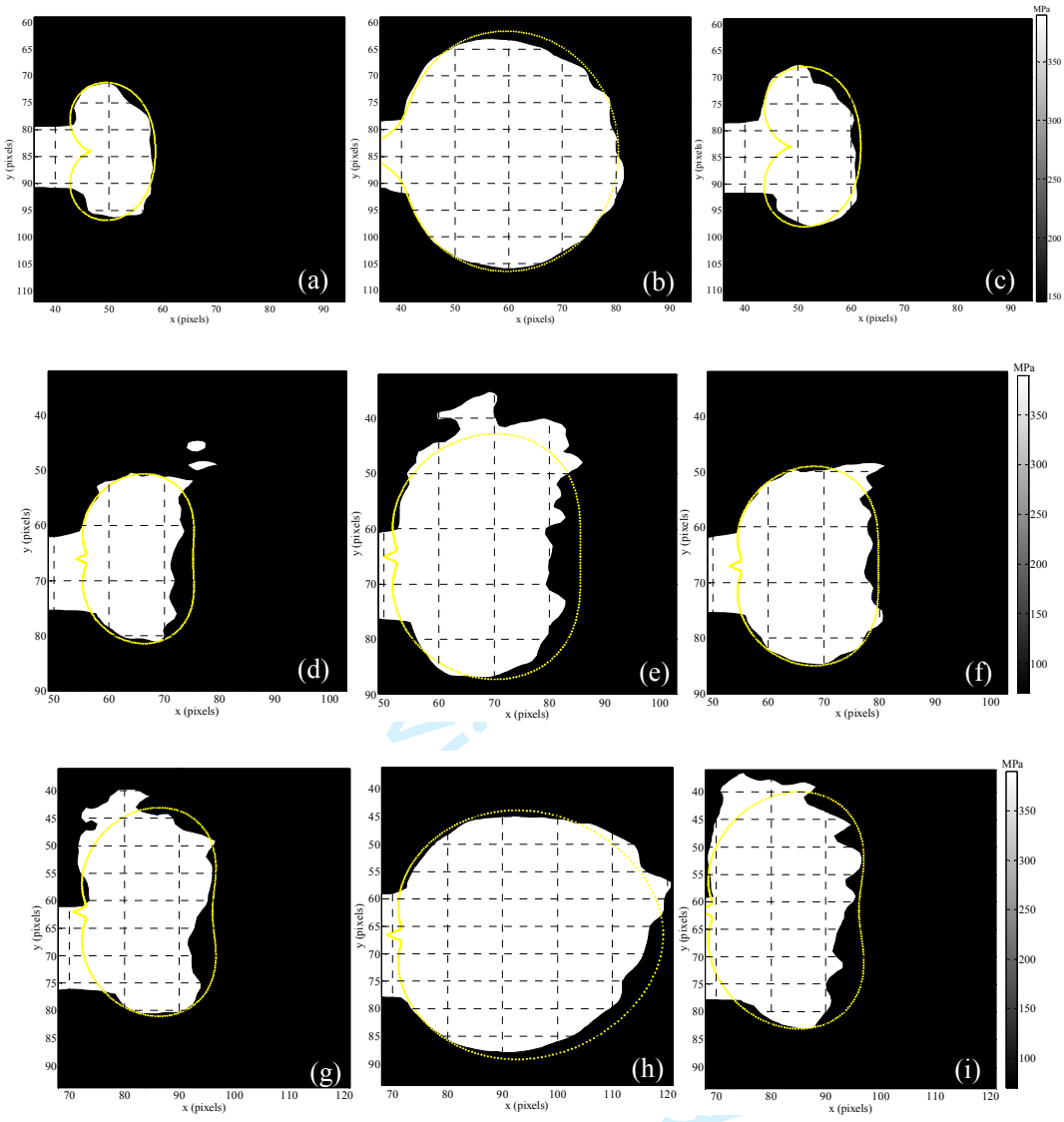

Figure 10 Comparison between the experimental and predicted plastic zone size and shape obtained from the application of overload cycles. CT1 specimen: (a) prior to, (b) after the overload cycle and (c) after the cycle immediately following the overload. CT2 specimen 20% overload: (d) prior to, (e) after the overload cycle and (f) after the cycle immediately following the overload. CT2 specimen 50% overload:(g) prior to, (h) after the overload cycle and (i) after the cycle immediately following the overload

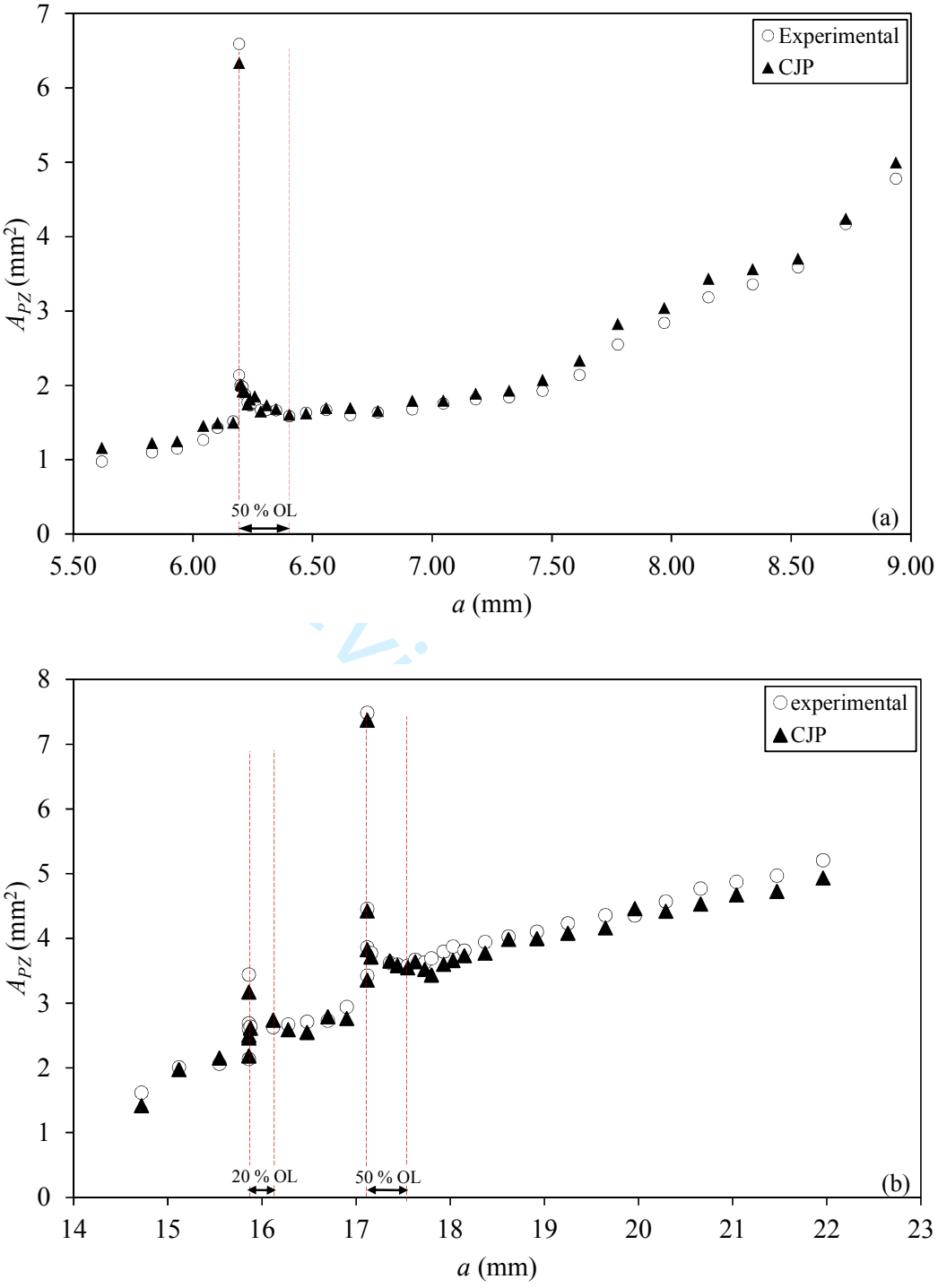

Figure 11 Comparison between the experimental and CJP predictions of plastic zone area as a function of the crack length for both specimens: (a) CT1 specimen and (b) CT2 specimen.

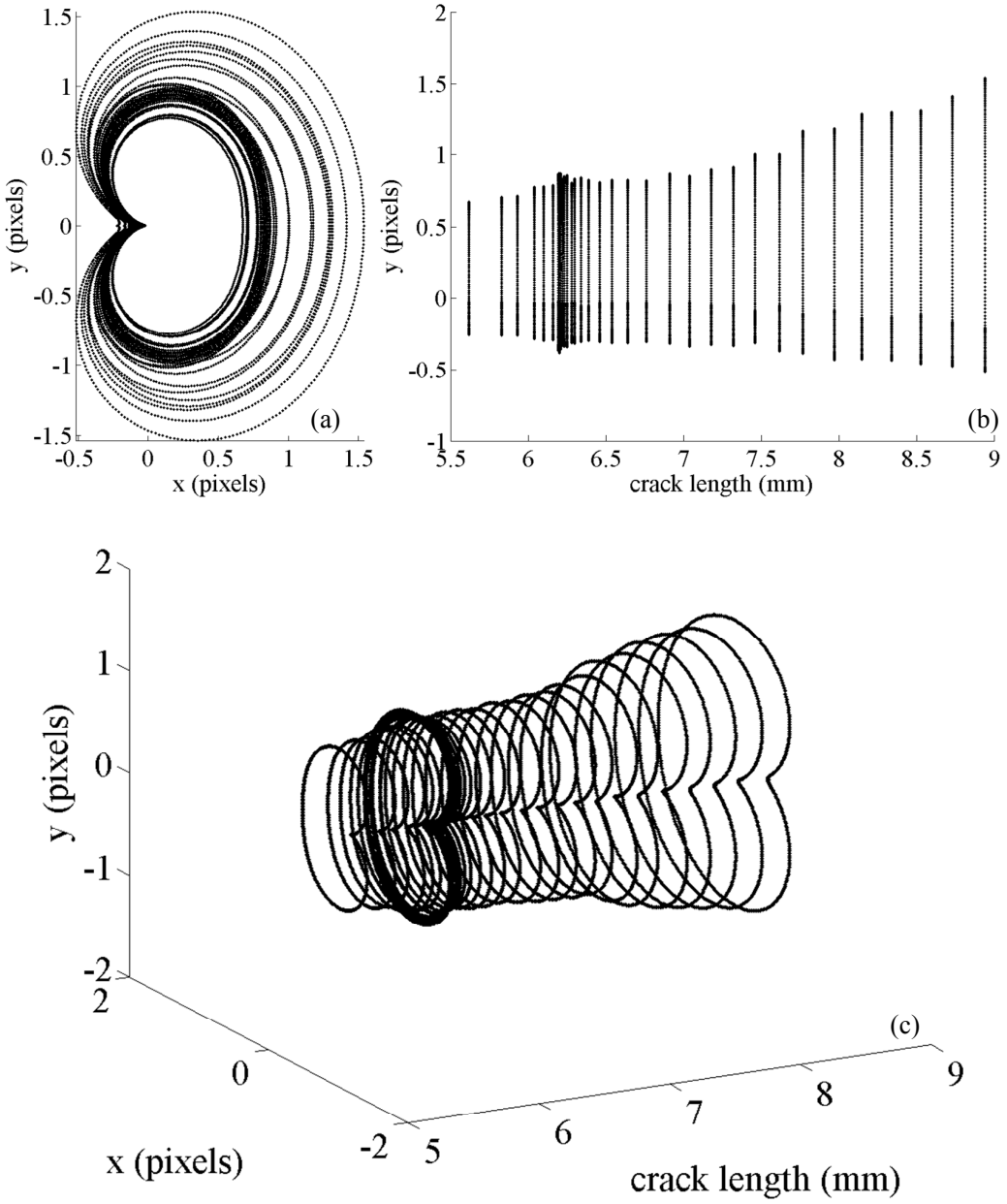

Figure 12 Illustration of the evolution of the crack tip plastic zone dimensions predicted by the CJP model as a function of crack length in the CT1 specimen. (a) and (b) 2D views, (c) 3D view.

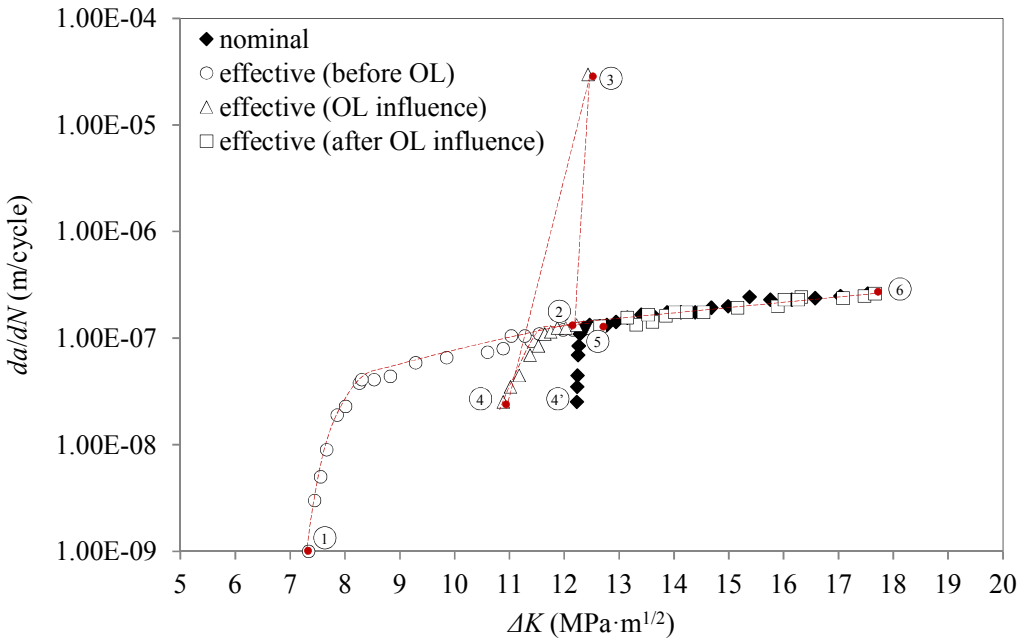

Figure 13 Fatigue crack growth rate as a function of the stress intensity factor range for the CT1 specimen. The data for ΔK_{eff} are represented by white symbols and the data for ΔK_{nom} after the application of the overload are shown by black symbols. The various stages in the evolution of the fatigue crack growth rate are indicated by numbers and explained in the text of the paper.

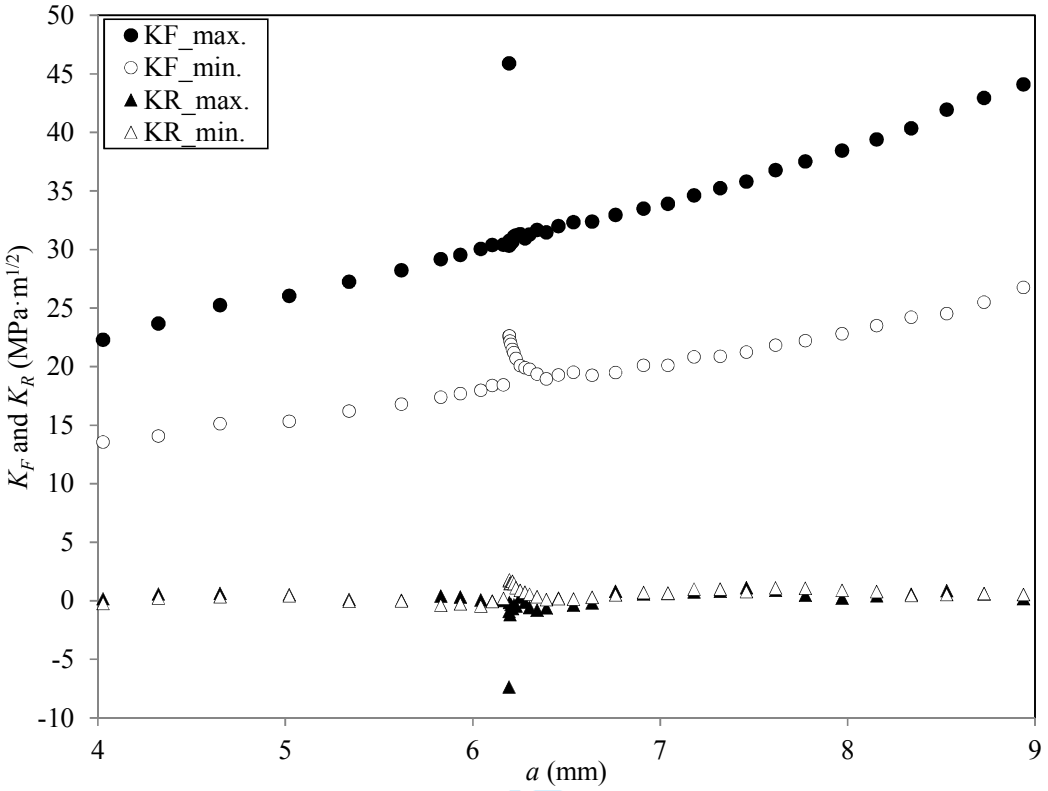

Figure 14 K_F and K_R stress intensity factor values as a function of crack length for the CT1 specimen.

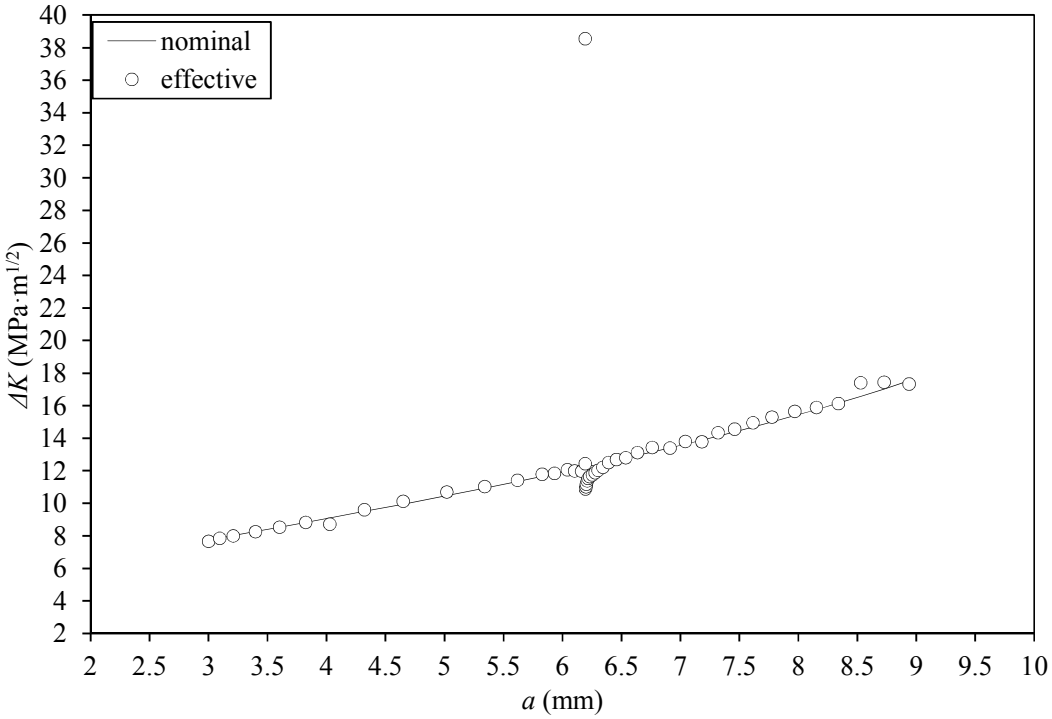

Figure 15 Effective stress intensity factor range [$\Delta K_{eff} = (K_F\text{-}K_R)_{max} - (K_F\text{-}K_R)_{min}$] as a function of the crack length. Nominal stress intensity data have been also plotted for comparative purposes.